# Can DOA Algorithms Be Deceived?

Licheng Zhao, Rui Zhou, Ming-Yi You, and Wenqiang Pu

***Abstract*—In this paper, we reflect on an interesting question whether direction of arrival (DOA) detection algorithms can be deceived. When the transmit signals are independent, prevalent DOA algorithms suffice to find the correct arriving directions from measurement statistics at the receiver end. But when the signals are coherent, the expected spectrum peaks may not show up and the detection performance deteriorates to a great extent. Instead of addressing the coherence issue, we take advantage of this phenomenon and fake a peak at a desired DOA in an attempt to launch a deception attack. The deception is realized by constructing a specified steering vector through a composite of candidate vectors in the dictionary. Thereafter, we apply the alternating direction method of multipliers (ADMM) framework to develop an efficient solution algorithm. Numerical simulations show that the proposed algorithm gives satisfactory DOA deception performance.**

***Index Terms*—DOA, deception attack, steering vector, ADMM.**

## I. Introduction

Array signal processing has been a fundamental research topic in the past few decades [1] and direction of arrival (DOA) estimation is one of the mainstream tasks in this well-studied area. In brief, DOA estimation aims to determine angular directions of the impinging signals using narrowband sensor arrays. The sensor array is assumed to be a uniform linear array (ULA). The array measurement model at time slot $t$ is denoted as

$$\mathbf{x}(t) = \mathbf{A}\mathbf{s}(t) + \mathbf{n}(t), \tag{1}$$

where $\mathbf{x}(t) \in \mathbb{C}^M$ is the received signal, $\mathbf{A} = [\mathbf{a}(\theta_1), \ldots, \mathbf{a}(\theta_N)] \in \mathbb{C}^{M\times N}$ is the array response matrix with $\mathbf{a}(\theta) \in \mathbb{C}^M$ being the steering vector, $\mathbf{s}(t) \in \mathbb{C}^N$ is the transmit signal waveform, and $\mathbf{n}(t) \in \mathbb{C}^M$ is an additive white Gaussian noise vector with zero mean and covariance $\sigma^2\mathbf{I}$. The covariance matrix of the received signal is given as

$$\mathbf{R} = \mathbf{A}\mathbf{P}\mathbf{A}^H + \sigma^2\mathbf{I} \tag{2}$$

with $\mathbf{P} = \mathbb{E}\left[\mathbf{s}(t)\mathbf{s}^H(t)\right]$. When the antennas are placed at half-wavelength spacing, the steering vector is expressed as $\mathbf{a}(\theta) = [1, \exp(j\pi\sin\theta), \ldots, \exp(j\pi(M-1)\sin\theta)]^T$. To estimate the parameter $\boldsymbol{\theta} = [\theta_1, \ldots, \theta_N]^T$ from the observed signals $\{\mathbf{x}(t)\}_{t=1}^T$, researchers have put forward numerous effective methods, of which Capon [2], MUSIC [3], ESPRIT [4], and SPARROW [5] are the most representative ones. Capon is a beamforming technique which minimizes the noise power subject to a fixed gain in the interested looking direction. MUSIC is a subspace-based method involving projection into the noise eigenspace of the sample covariance matrix. ESPRIT exploits the rotational invariance property in steering vector and performs singular value decomposition on the collected stacking samples. SPARROW is developed from a row-sparsity induced measurement sample fitting problem and adopts a coordinate descent scheme. However, all these algorithms may suffer performance degradation when the transmitted signals are coherent. Transmit signal coherence leads to rank deficiency in source covariance $\mathbf{P}$, which in turn causes noise subspace distortion. The spectrum peaks may be aliased at the DOA locations.

To address the coherence issue, existing literature concentrates on correlation reduction and several effective approaches have been proposed. Specially, in the case of two coherent transmit waveforms, a forward-backward averaging trick is employed [6]. When there exist more than two coherent sources, a spatial smoothing technique is invented to increase spectrum resolution. The entire ULA is divided into several overlapping subarrays and the covariance matrices retrieved from the subarrays are averaged to promote a random phase modulation [7]. But in this paper, we take a different perspective. Instead of distinguishing the DOAs of coherent signals, we try to fake a peak from those signals at a desired DOA and "deceive" the receiver nodes which use prevalent algorithms for DOA estimation. This technique is named DOA deception and is based on a simpler array measurement model than (1), which is

$$\mathbf{x}(t) = [\mathbf{D}_\mathbf{A}\mathbf{p}]\, s(t) + \mathbf{n}(t) \approx \mathbf{a}(\theta)\, s(t) + \mathbf{n}(t). \tag{3}$$

The spectrum peak results from an almost equivalent steering vector $\mathbf{a}(\theta)$ constructed by a linear combination of some candidate vectors in the dictionary, i.e., $\mathbf{D}_\mathbf{A}\mathbf{p}$, where $\mathbf{D}_\mathbf{A} = [\mathbf{a}(\theta_1), \ldots, \mathbf{a}(\theta_{N_D})] \in \mathbb{C}^{M\times N_D}$, $\Theta_N = \{\theta_n\}_{n=1}^{N_D}$ is a sorted set of uniformly spaced grids in $[-90°, 90°)$, and $\mathbf{p} \in \mathbb{C}^{N_D}$ is the combination weight. Note that the columns of $\mathbf{D}_\mathbf{A}$ are not linearly independent, so it holds true mathematically that one steering vector could be a linear combination of the other steering vectors in $\mathbf{D}_\mathbf{A}$.

This technique may be useful in providing protection for critical electronic infrastructure like communication nodes. Compared with existing deception techniques in radar countermeasures, e.g., active decoy (drawing an enemy away from an important target) [8, 9] and centroid jamming (disrupting the calculation of the target geometric center) [10, 11], the deception scheme of (3) stems from a signal-reconstruction point of view, while the existing techniques [8, 9, 10, 11] utilize auxiliary objects, such as decoys and chaff, to fulfill the deception purpose.

The contributions of this paper are listed as follows. Firstly, we take a new perspective on signal coherence. We exploit this phenomenon and propose a method to fool a receiver

This work was supported in part by the National Nature Science Foundation of China (NSFC) under Grant 62206182, 62101350, and 62201362, and in part by the Guangdong Basic and Applied Basic Research Foundation under Grant 2024A1515010154.

Licheng Zhao, Rui Zhou, and Wenqiang Pu are with Shenzhen Research Institute of Big Data, Shenzhen 518172, China (email: {zhaolicheng, rui.zhou, wpu}@sribd.cn). Ming-Yi You is with the National Key Laboratory of Electromagnetic Space Security, Jiaxing, China (e-mail: youmingyi@126.com). (*Corresponding author: Wenqiang Pu.*)

node with an illusion of a false peak at a given DOA. This is an area rarely explored in the open literature. To the best of our knowledge, we are the first to systematically explore the possibility of deception in DOA estimation. Secondly, we formulate our method into an optimization problem and develop an efficient solution algorithm based on alternating direction method of multipliers (ADMM) to select the proper steering vector candidates and generate the combination weights.

## II. Problem Formulation

Given the steering vector candidates and the combination weights, the DOA deception method is to place synchronized emission sources at the selected DOA directions with an equal distance to the receiver node. The emission sources form a semicircle topology. The transmit signals are coherent subject to power amplification and phase shifting instructed by the assigned combination weight. Hence, the key step of the DOA deception method is to fit the steering vector combination $\mathbf{D_A p}$ to the desired target vector $\mathbf{a}(\theta)$. In engineering practice, there could be additional requirements in the fitting design. Firstly, to cater for the slight uncertainty in the nominal target DOA, we incorporate a set of target vectors, $\{\mathbf{a}(\theta_i)\}_{i=1}^I$, with $\Theta_I = \{\theta_i\}_{i=1}^I$ covering the entire uncertainty range of $\theta$. Secondly, to avoid position exposure, emission sources should be placed several degrees away from the nominal DOA, and thus $p_n = 0$, $\forall n \in \{n \,|\, |\theta_n - \theta| \le c, \theta_n \in \Theta_N\} = \mathcal{N}_0$, where $p_n$ is the n-th element of $\mathbf{p}$, $c$ is the threshold parameter to describe the range of the angular danger zone, and $\Theta_N$ is the set of spaced grids defined in Section I, below equation (3). Lastly, it is financially unaffordable to deploy too many transmitters, so the number of nonzero elements in $\mathbf{p}$ should not exceed an upper limit $K$. Considering all the requirements above, we formulate the optimization problem as

$$\begin{aligned} \underset{\mathbf{p}}{\text{minimize}} \quad & \max_{i=1,\dots,I} \|\mathbf{a}(\theta_i) - \mathbf{D_A p}\|_2 \\ \text{subject to} \quad & p_n = 0, \forall n \in \mathcal{N}_0 \\ & \|\mathbf{p}\|_0 \le K. \end{aligned} \tag{4}$$

The objective adopts a minimax scheme to provide a worst-case guarantee against target uncertainty. The fitting metric is chosen as the Euclidean distance. The optimized variable has a mandatory zero-valued region and the cardinality, characterized by the $\ell_0$ norm, is no more than $K$.

*Remark* 1. Given $\mathbf{D_A} \in \mathbb{C}^{M \times N_D}$ with $N_D \gg M$, as $K$ increases such that $K \ge M$, there exists a column $\mathbf{a}(\bar{\theta}_n)$ and a weight vector $\bar{\mathbf{p}}$ such that $\bar{\mathbf{D}}_\mathbf{A}\bar{\mathbf{p}} = \mathbf{a}(\bar{\theta}_n)$ and $\|\bar{\mathbf{p}}\|_0 \le K$ ($\bar{\mathbf{D}}_\mathbf{A}$ is constructed from $\mathbf{D_A}$ excluding $\mathbf{a}(\bar{\theta}_n)$). The nonzero elements of $\bar{\mathbf{p}}$ are placed on the indices of the maximal linearly independent system of $\bar{\mathbf{D}}_\mathbf{A}$.

## III. DOA Deception Algorithm

First, we recast problem (4) into the epigraph form as (5):

$$\begin{aligned} \underset{\mathbf{p},t}{\text{minimize}} \quad & t \\ \text{subject to} \quad & \|\mathbf{a}(\theta_i) - \mathbf{D_A p}\|_2 \le t, \ i = 1, \dots, I \\ & p_n = 0, \forall n \in \mathcal{N}_0 \\ & \|\mathbf{p}\|_0 \le K. \end{aligned} \tag{5}$$

Next, we introduce auxiliary variables $\{\mathbf{z}_i\}_{i=1}^I$ and $\{t_i\}_{i=1}^I$ to fully decouple the first constraint:

$$\begin{aligned} \underset{\mathbf{p},t,\{\mathbf{z}_i,t_i\}}{\text{minimize}} \quad & t \\ \text{subject to} \quad & \mathbf{z}_i = \mathbf{a}(\theta_i) - \mathbf{D_A p}, \ i = 1, \dots, I \\ & t_i = t, \ i = 1, \dots, I \\ & \|\mathbf{z}_i\|_2 \le t_i, \ i = 1, \dots, I \\ & p_n = 0, \forall n \in \mathcal{N}_0 \\ & \|\mathbf{p}\|_0 \le K. \end{aligned} \tag{6}$$

Then we solve the optimization problem (6) under the ADMM framework. The (partial) augmented Lagrangian is given by

$$\begin{aligned} \mathcal{L}(\mathbf{p}, t, \{\mathbf{z}_i, t_i\}, \{\boldsymbol{\lambda}_i, \mu_i\}) &= t + \left( \sum_{i=1}^I \mathrm{Re}\left[ \boldsymbol{\lambda}_i^H (\mathbf{z}_i - (\mathbf{a}(\theta_i) - \mathbf{D_A p})) \right] \right) \\ &+ \frac{\rho}{2} \left( \sum_{i=1}^I \|\mathbf{z}_i - (\mathbf{a}(\theta_i) - \mathbf{D_A p})\|_2^2 \right) \\ &+ \left( \sum_{i=1}^I \mu_i (t - t_i) \right) + \frac{\rho}{2} \left( \sum_{i=1}^I (t - t_i)^2 \right) \end{aligned} \tag{7}$$

where $\mathbf{p}$, $t$, and $\{\mathbf{z}_i, t_i\}$ are primal variables and $\{\boldsymbol{\lambda}_i, \mu_i\}$ are dual variables with respect to the constraints $\mathbf{z}_i = \mathbf{a}(\theta_i) - \mathbf{D_A p}$ and $t_i = t$. To fit in the ADMM convergence framework by Wang et al. [12], the variable updates are organized in the following way: (for simple notation, the updated variable is marked with a superscript "+")

$$\begin{cases} \left(\mathbf{z}_i^+, t_i^+\right) = \arg\min_{\|\mathbf{z}_i\|_2 \le t_i} \mathcal{L}(\mathbf{p}, t, \{\mathbf{z}_i, t_i\}, \{\boldsymbol{\lambda}_i, \mu_i\}), \forall i \\ \mathbf{p}^+ = \arg\min_{p_n = 0, \forall n \in \mathcal{N}_0, \|\mathbf{p}\|_0 \le K} \mathcal{L}(\mathbf{p}, t, \{\mathbf{z}_i, t_i\}, \{\boldsymbol{\lambda}_i, \mu_i\}) \\ t^+ = \arg\min_t \mathcal{L}(\mathbf{p}, t, \{\mathbf{z}_i, t_i\}, \{\boldsymbol{\lambda}_i, \mu_i\}) \\ \boldsymbol{\lambda}_i^+ = \boldsymbol{\lambda}_i + \rho(\mathbf{z}_i - (\mathbf{a}(\theta_i) - \mathbf{D_A p})), \forall i \\ \mu_i^+ = \mu_i + \rho(t - t_i), \forall i. \end{cases} \tag{8}$$

In what follows, we solve the minimization subproblems in the ADMM steps. We start with the simple update of $t^+$:

$$\begin{aligned} t^+ &= \arg\min_t \mathcal{L}(\mathbf{p}, t, \{\mathbf{z}_i, t_i\}, \{\boldsymbol{\lambda}_i, \mu_i\}) \\ &= \arg\min_t \left\{ t + \left[ \sum_{i=1}^I \left( \mu_i (t - t_i) + \frac{\rho}{2} (t - t_i)^2 \right) \right] \right\} \\ &= \frac{1}{I} \left( \sum_{i=1}^I t_i \right) - \frac{1}{\rho I} \left[ 1 + \left( \sum_{i=1}^I \mu_i \right) \right]. \end{aligned} \tag{9}$$

Then we study the update of $(\mathbf{z}_i, t_i)$:

$$\begin{aligned} &\left(\mathbf{z}_i^+, t_i^+\right) = \arg\min_{\|\mathbf{z}_i\|_2 \le t_i} \mathcal{L}(\mathbf{p}, t, \{\mathbf{z}_i, t_i\}, \{\boldsymbol{\lambda}_i, \mu_i\}) \\ &= \arg\min_{\|\mathbf{z}_i\|_2 \le t_i} \frac{2}{\rho} \mathrm{Re}\left[ \boldsymbol{\lambda}_i^H (\mathbf{z}_i - \mathbf{b}_i) \right] + \|\mathbf{z}_i - \mathbf{b}_i\|_2^2 \\ &\qquad - \frac{2}{\rho} \mu_i t_i + (t_i - t)^2 \\ &= \arg\min_{\|\mathbf{z}_i\|_2 \le t_i} \left\| \begin{bmatrix} \mathbf{z}_i \\ t_i \end{bmatrix} - \begin{bmatrix} \mathbf{b}_i - \frac{1}{\rho}\boldsymbol{\lambda}_i \\ t + \frac{1}{\rho}\mu_i \end{bmatrix} \right\|_2^2 \\ &= \begin{cases} (\mathbf{0}, 0) & \left\| \mathbf{b}_i - \frac{1}{\rho}\boldsymbol{\lambda}_i \right\|_2 \le -\left( t + \frac{1}{\rho}\mu_i \right) \\ \left( \mathbf{b}_i - \frac{1}{\rho}\boldsymbol{\lambda}_i, t + \frac{1}{\rho}\mu_i \right) & \left\| \mathbf{b}_i - \frac{1}{\rho}\boldsymbol{\lambda}_i \right\|_2 \le t + \frac{1}{\rho}\mu_i \\ \frac{1}{2}\left( 1 + \frac{t + \frac{1}{\rho}\mu_i}{\left\| \mathbf{b}_i - \frac{1}{\rho}\boldsymbol{\lambda}_i \right\|_2} \right) \cdot & \text{otherwise} \\ \left( \mathbf{b}_i - \frac{1}{\rho}\boldsymbol{\lambda}_i, \left\| \mathbf{b}_i - \frac{1}{\rho}\boldsymbol{\lambda}_i \right\|_2 \right) \end{cases} \end{aligned} \tag{10}$$

where $\mathbf{b}_i = \mathbf{a}(\theta_i) - \mathbf{D_A p}$. The underlying geometric intuition of (10) can be described as a projection onto the standard

second-order cone [13, 6.3.2]. Finally, we attend to the update of $\mathbf{p}$. Let $\mathcal{P}=\{\mathbf{p}|p_n=0,\forall n\in\mathcal{N}_0,\|\mathbf{p}\|_0\leq K\}$, and we have

$$\begin{aligned}\mathbf{p}^+&=\arg\min_{\mathbf{p}\in\mathcal{P}}\mathcal{L}\left(\mathbf{p},t,\{\mathbf{z}_i\},\{\boldsymbol{\lambda}_i\}\right)\\&=\arg\min_{\mathbf{p}\in\mathcal{P}}\left[\sum_{i=1}^{I}\left(\frac{2}{\rho}\mathrm{Re}\left[\boldsymbol{\lambda}_i^H\mathbf{D}_\mathbf{A}\mathbf{p}\right]+\|\mathbf{D}_\mathbf{A}\mathbf{p}-\mathbf{c}_i\|_2^2\right)\right]\\&=\arg\min_{\mathbf{p}\in\mathcal{P}}\mathbf{p}^H\mathbf{D}_\mathbf{A}^H\mathbf{D}_\mathbf{A}\mathbf{p}-\frac{2}{I}\mathrm{Re}\left[\sum_{i=1}^{I}\left(\left(\mathbf{c}_i-\frac{1}{\rho}\boldsymbol{\lambda}_i\right)^H\mathbf{D}_\mathbf{A}\mathbf{p}\right)\right]\end{aligned}\tag{11}$$

where $\mathbf{c}_i=\mathbf{a}\left(\theta_i\right)-\mathbf{z}_i$. Given an arbitrary quadratic function, minimization on constraint set $\mathcal{P}$ does not yield a closed-form solution. For the sake of algorithmic simplicity, we construct a tight upper bound of the original quadratic function and minimize the surrogate function to get a closed-form update. This idea originates from the majorization-minimization (MM) framework [14] and a feasible crossover between ADMM and MM can be found in [15]. Referring to [16], a tight upper bound of $\mathbf{p}^H\mathbf{D}_\mathbf{A}^H\mathbf{D}_\mathbf{A}\mathbf{p}$ at $\mathbf{p}=\mathbf{p}_0$ is constructed as

$$\mathbf{p}^H\mathbf{D}_\mathbf{A}^H\mathbf{D}_\mathbf{A}\mathbf{p}\leq\bar{\lambda}\cdot\mathbf{p}^H\mathbf{p}-2\mathrm{Re}\left[\mathbf{p}^H\mathbf{G}\mathbf{p}_0\right]+\mathbf{p}_0^H\mathbf{G}\mathbf{p}_0,\tag{12}$$

where $\bar{\lambda}=\lambda_{\max}\left(\mathbf{D}_\mathbf{A}^H\mathbf{D}_\mathbf{A}\right)$ and $\mathbf{G}=\lambda_{\max}\left(\mathbf{D}_\mathbf{A}^H\mathbf{D}_\mathbf{A}\right)\mathbf{I}-\mathbf{D}_\mathbf{A}^H\mathbf{D}_\mathbf{A}$. Thus, the upper bound surrogate function for $\mathbf{p}$ update

$$\begin{aligned}f\left(\mathbf{p},\mathbf{p}_0\right)=&\bar{\lambda}\cdot\mathbf{p}^H\mathbf{p}-2\mathrm{Re}\left[\mathbf{p}^H\mathbf{G}\mathbf{p}_0\right]+\mathbf{p}_0^H\mathbf{G}\mathbf{p}_0\\&-\frac{2}{I}\mathrm{Re}\left[\sum_{i=1}^{I}\left(\left(\mathbf{c}_i-\frac{1}{\rho}\boldsymbol{\lambda}_i\right)^H\mathbf{D}_\mathbf{A}\mathbf{p}\right)\right].\end{aligned}\tag{13}$$

We continue with the update of $\mathbf{p}$:

$$\begin{aligned}\mathbf{p}^+&=\arg\min_{\mathbf{p}\in\mathcal{P}}f\left(\mathbf{p},\mathbf{p}_0\right)\\&\overset{(a)}{=}\arg\min_{\mathbf{p}\in\mathcal{P}}\|\mathbf{p}-\mathbf{d}\|_2^2\overset{(b)}{=}\begin{cases}d_n & n\in\mathcal{N}_K\\0 & n\notin\mathcal{N}_K\end{cases}.\end{aligned}\tag{14}$$

where (a) is because $f\left(\mathbf{p},\mathbf{p}_0\right)=\bar{\lambda}\cdot\|\mathbf{p}-\mathbf{d}\|_2^2-\bar{\lambda}\cdot\mathbf{d}^H\mathbf{d}+\mathbf{p}_0^H\mathbf{G}\mathbf{p}_0$ with $\mathbf{d}=\left[\mathbf{G}\mathbf{p}_0+\mathbf{D}_\mathbf{A}^H\cdot\frac{1}{I}\left(\sum_{i=1}^{I}\left(\mathbf{c}_i-\frac{1}{\rho}\boldsymbol{\lambda}_i\right)\right)\right]/\bar{\lambda}$, and (b): $\mathcal{N}_K=\left\{n\middle||d_n|\geq\tilde{\mathbf{d}}_{[K]},n\notin\mathcal{N}_0\right\}$, $\tilde{\mathbf{d}}=|\mathbf{d}\left[n\notin\mathcal{N}_0\right]|$, and $\tilde{\mathbf{d}}_{[n]}$ denotes the $n$-th largest component of $\tilde{\mathbf{d}}$. To this point, we can summarize the DOA Deception Algorithm, as in Algorithm 1. The per-iteration computational complexity is $\mathcal{O}\left(MN_D\right)$, resulting from the matrix-vector multiplication. The convergence behavior of Algorithm DDA inherits from the general framework of [12] and a majorization in Lagrangian does not change the monotonic descent property throughout the proof.

The computational complexity analysis is carried out on a per-iteration basis. The dominating operation in the update of $\left(\mathbf{z}_i^{(k+1)},t_i^{(k+1)}\right)$ is $\mathbf{D}_\mathbf{A}\mathbf{p}^{(k)}$, of complexity $\mathcal{O}\left(MN_D\right)$. The dominating operations in the update of $\mathbf{p}^{(k+1)}$ are $\mathbf{D}_\mathbf{A}^H\left(\mathbf{D}_\mathbf{A}\mathbf{p}^{(k)}\right)$ and $\mathbf{D}_\mathbf{A}^H\cdot\frac{1}{I}\left(\sum_{i=1}^{I}\left(\mathbf{c}_i-\frac{1}{\rho}\boldsymbol{\lambda}_i^{(k)}\right)\right)$, both of complexity $\mathcal{O}\left(MN_D\right)$ when calculated in a proper order. The computational complexity in the update of $t^{(k+1)}$ is $\mathcal{O}\left(1\right)$. The dominating operation in the update of $\boldsymbol{\lambda}_i^{(k+1)}$ is $\mathbf{D}_\mathbf{A}\mathbf{p}^{(k+1)}$, of complexity $\mathcal{O}\left(MN_D\right)$. The computational complexity in the update of $\mu_i^{(k+1)}$ is $\mathcal{O}\left(1\right)$. Therefore, the per-iteration complexity of the proposed algorithm is $\mathcal{O}\left(MN_D\right)$.

**Algorithm 1** DOA Deception Algorithm (DDA).

**Require:** Input: $\mathbf{D}_\mathbf{A}$, $\Theta_I$, $\mathcal{N}_0$, and $K$. Iteration count $k=0$. Initialize $t^{(0)}$, $\mathbf{p}^{(0)}$, $\left\{\mathbf{z}_i^{(0)}\right\}$, $\left\{t_i^{(0)}\right\}$, $\left\{\boldsymbol{\lambda}_i^{(0)}\right\}$, and $\left\{\mu_i^{(0)}\right\}$. Set $\rho=0.01$.

$l_{\max}=\|\mathbf{D}_\mathbf{A}\|_2^2$ (squared spectral norm);
**repeat**
  $\mathbf{b}_i=\mathbf{a}\left(\theta_i\right)-\mathbf{D}_\mathbf{A}\mathbf{p}^{(k)}$, $\forall i$;
  $\left(\mathbf{z}_i^{(k+1)},t_i^{(k+1)}\right)$ follow eq. (10), $\forall i$;
  $\mathbf{c}_i=\mathbf{a}\left(\theta_i\right)-\mathbf{z}_i^{(k+1)}$, $\forall i$;
  $\mathbf{d}=\left[l_{\max}\cdot\mathbf{p}^{(k)}-\mathbf{D}_\mathbf{A}^H\left(\mathbf{D}_\mathbf{A}\mathbf{p}^{(k)}\right)+\mathbf{D}_\mathbf{A}^H\cdot\frac{1}{I}\left(\sum_{i=1}^{I}\left(\mathbf{c}_i-\frac{1}{\rho}\boldsymbol{\lambda}_i^{(k)}\right)\right)\right]/l_{\max}$;
  $\tilde{\mathbf{d}}=|\mathbf{d}\left[n\notin\mathcal{N}_0\right]|$ and obtain $\mathcal{N}_K=\left\{n\middle||d_n|\geq\tilde{\mathbf{d}}_{[K]},n\notin\mathcal{N}_0\right\}$;
  $\mathbf{p}^{(k+1)}=\begin{cases}d_n & n\in\mathcal{N}_K\\0 & n\notin\mathcal{N}_K\end{cases}$;
  $t^{(k+1)}=\frac{1}{I}\left(\sum_{i=1}^{I}t_i^{(k+1)}\right)-\frac{1}{\rho I}\left[1+\left(\sum_{i=1}^{I}\mu_i^{(k)}\right)\right]$;
  $\boldsymbol{\lambda}_i^{(k+1)}=\boldsymbol{\lambda}_i^{(k)}+\rho\left(\mathbf{z}_i^{(k+1)}-\left(\mathbf{a}\left(\theta_i\right)-\mathbf{D}_\mathbf{A}\mathbf{p}^{(k+1)}\right)\right)$ and $\mu_i^{(k+1)}=\mu_i^{(k)}+\rho\left(t^{(k+1)}-t_i^{(k+1)}\right)$, $\forall i$;
  $k=k+1$;
**until** objective change $<\varepsilon$ ($\varepsilon=10^{-6}$ by default)

*Remark* 2 *Source Deployment Tips.* Apart from the semicircle topology, the emission sources could be deployed with other topological structures as long as the arriving signals at the receiver end are completely coherent. To ensure coherence, the signal time frames are moved forward or delayed backward in comparison to the reference node. The number of frames to be shifted is determined by the distance difference (to the receiver) $\Delta r$ and sampling frequency $f_s$, and calculated as $f_s\cdot\Delta r/c$ ($c$ is the speed of light). In practical deployment, $\Delta r$ can be designed such that $f_s\cdot\Delta r/c$ is an integer. In face of imperfect synchronization, we could transmit slow-varying codes so that the sampling frequency can be lowered and that the offset becomes negligible. In view of imprecise amplitude/phase control, we could consider worst-case robust optimization.

## IV. Numerical Simulations

In this section, we present numerical results for the proposed DOA deception method. All simulations are performed on a PC with a 2.90 GHz i7-10700 CPU and 16.0 GB RAM. We set $M=10$, $\Theta_N=\{-90°,-89°,\ldots,89°\}$, and thus $\mathbf{D}_\mathbf{A}\in\mathbb{C}^{10\times180}$. The nominal target DOA $\theta$ is $60°$ and $\Theta_I$ is specified as $\{60°\pm3°\}$. The zero-valued index set $\mathcal{N}_0$ is $\{n\,|\,|\theta_n-60°|\leq10°,\theta_n\in\Theta_N\}$. The number of transmit sources deployed $K$ is 10 by default and could be varied upon request. The signal-to-noise-ratio (SNR) is 0dB at the receiver node. The DOA detection algorithms are Capon, MUSIC, ESPRIT, and spatial smoothing, as mentioned in Sec. I.

When $K$ is fixed at the default value, the source deployment solution produced by DDA is presented in Figure 1a. The transmit power and phase attenuation information is contained in the combination weight output. For safety reasons, it is not allowed to place any sources in the shaded area, so the transmitters are scattered on the two sides, one on the right and nine on the left. To avoid temporal asynchrony, the

This article has been accepted for publication in IEEE Signal Processing Letters. This is the author's version which has not been fully edited and content may change prior to final publication. Citation information: DOI 10.1109/LSP.2025.3576679



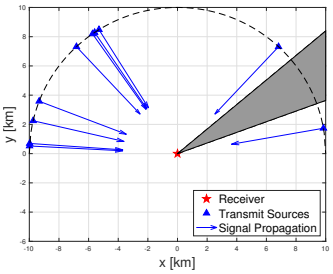


(a) Source deployment layout.

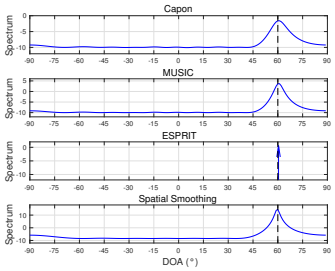


(b) DOA spectrum of different detection algorithms with $K = 10$.

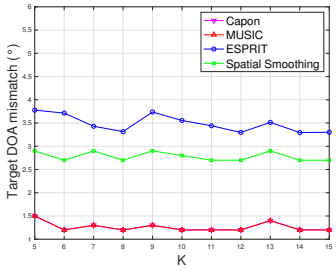


(c) Target DOA mismatch versus $K$.

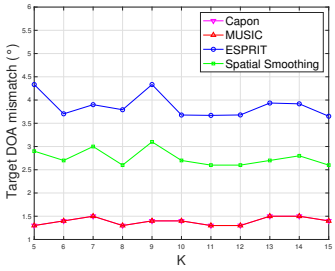


(d) Target DOA mismatch versus $K$ under random phase drifts.

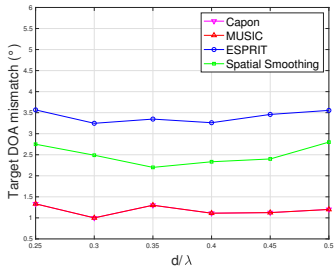


(e) Target DOA mismatch in degree versus different choices of $d/\lambda$.

Figure 1: Miscellaneous numerical results.

topology of source placement is designated as a semicircle. As a verification of the deception performance, we present the DOA spectrum plots of different detection algorithms in Figure 1b. The black dashed line indicates the nominal target DOA. Conditioned on the scene of DDA output, all the four detection algorithms generate a spectral peak or give an estimation result very close to the target DOA. This phenomenon implies a success in DOA deception.

When the value of $K$ is varied among $\{5, 6, \ldots, 15\}$, we study the average angular mismatch between the estimated and target DOA. The estimated DOA is denoted as $\theta_{\text{est}}$ and the target DOA is represented by $\theta_{\text{tar}}$. DOA mismatch is formally defined as their absolute difference: $|\theta_{\text{est}} - \theta_{\text{tar}}|$. The simulation results are displayed in Figure 1c. Each reported data point is averaged over 30 random initialization instances. The detection results of Capon and MUSIC are less than $1.5°$ away from the target DOA while those of Spatial Smoothing and ESPRIT are less than $3°$ and $4°$ across the entire range of $K$. We can observe a steady trend of DOA mismatch as $K$ increases. The primary reason for this steady trend is that, through the strategic deployment of a sufficient number of coherent signal sources (e.g., $K = 5$), the received array signal can effectively emulate a single-source impinging signal from a deceptive angular direction. Further increasing the value of $K$ yields minimal improvement in deception performance. Overall, the deception performance could be considered satisfactory.

Next, we consider a practical issue of imperfect signal coherence among different transmitters. This issue is caused by non-ideal digital-to-analogue modules and the consequence is a random phase drift on the original signal. In this experiment, the phase drifts at the transmit sources are assumed as independent and identically uniformly-distributed random variables $\mathcal{U}\left(-5^{\circ}, 5^{\circ}\right)$. Then we rederive the angular mismatch simulation results. As can be seen in Figure 1d, the detection results very much resemble those of Figure 1c. The DOA mismatch occasionally exceeds the previous borderline by a narrow margin, indicating the robustness of DDA outputs against moderate random phase drifts at transmitters.

Finally, we investigate into the influence of the spacing factor in a uniform linear array. To avoid spatial aliasing, the element spacing $d$ should not exceed the half-wavelength distance $(\lambda/2)$. Thus, we vary $d/\lambda$ among $\{0.25, 0.3, \ldots, 0.5\}$. The source number $K$ is fixed as 10. The deception performance is presented in Figure 1e. The DOA mismatch levels of Capon and MUSIC are within $[1°, 1.5°]$ while those of Spatial Smoothing and ESPRIT are around $2.5°$ and $3.5°$. Hence, we can conclude that the deception performance is not so sensitive to the spacing factor.

## V. Conclusion

In this paper, we have studied the feasibility of DOA algorithm deception. By transmitting coherent signals at scattered emission sources, the prevalent DOA algorithms may not be able to distinguish the true arriving directions. This phenomenon enables DOA deception and it is possible to fake a spectral peak at a desired DOA. The deception technique is to construct an almost equivalent steering vector from a composite of candidate vectors in the dictionary. We have formulated the construction process into an optimization problem and proposed an efficient iterative algorithm based on the ADMM framework. The proposed algorithm has demonstrated a source deployment solution and the DOA deception performance has proved to be satisfactory. A promising future research avenue could be DOA anti-fraud defense.

## REFERENCES


[1] H. Krim and M. Viberg, "Two decades of array signal processing research: the parametric approach," *IEEE Signal Process. Mag.*, vol. 13, no. 4, pp. 67–94, 1996.

[2] J. Capon, "High-resolution frequency-wavenumber spectrum analysis," *Proc. IEEE*, vol. 57, no. 8, pp. 1408–1418, 1969.

[3] R. Schmidt, "Multiple emitter location and signal parameter estimation," *IEEE Trans. Antennas Propag.*, vol. 34, no. 3, pp. 276–280, 1986.

[4] R. Roy and T. Kailath, "Esprit-estimation of signal parameters via rotational invariance techniques," *IEEE Trans. Acoust., Speech, Signal Process.*, vol. 37, no. 7, pp. 984–995, 1989.

[5] C. Steffens, M. Pesavento, and M. E. Pfetsch, "A compact formulation for the $\ell_{2,1}$ mixed-norm minimization problem," *IEEE Trans. Signal Process.*, vol. 66, no. 6, pp. 1483–1497, 2018.

[6] S. U. Pillai and B. H. Kwon, "Forward/backward spatial smoothing techniques for coherent signal identification," *IEEE Trans. Acoust., Speech, Signal Process.*, vol. 37, no. 1, pp. 8–15, 1989.

[7] T.-J. Shan, M. Wax, and T. Kailath, "On spatial smoothing for direction-of-arrival estimation of coherent signals," *IEEE Trans. Acoust., Speech, Signal Process.*, vol. 33, no. 4, pp. 806–811, 1985.

[8] E. V. Lakshmi, N. Sastry, and B. P. Rao, "Optimum active decoy deployment for effective deception of missile radars," in *Proceedings of IEEE CIE International Conference on Radar*, vol. 1. IEEE, 2011, pp. 234–237.

[9] J.-W. Rim, I.-S. Koh, and S.-H. Choi, "Jamming performance analysis for repeater-type active decoy against ground tracking radar considering dynamics of platform and decoy," in *18th International Radar Symposium (IRS)*. IEEE, 2017, pp. 1–9.

[10] Y. Yang, D.-J. Feng, W.-M. Zhang, X.-S. Wang, and S.-P. Xiao, "Detection of chaff centroid jamming aided by GPS/INS," *IET Radar, Sonar & Navigation*, vol. 7, no. 2, pp. 130–142, 2013.

[11] Y. Yang, S.-P. Xiao, D.-J. Feng, and X.-S. Wang, "Polarisation oblique projection for radar seeker tracking in chaff centroid jamming environment without prior knowledge," *IET Radar, Sonar & Navigation*, vol. 8, no. 9, pp. 1195–1202, 2014.

[12] Y. Wang, W. Yin, and J. Zeng, "Global convergence of admm in nonconvex nonsmooth optimization," *Journal of Scientific Computing*, vol. 78, pp. 29–63, 2019.

[13] N. Parikh and S. Boyd, "Proximal algorithms," *Foundations and trends® in Optimization*, vol. 1, no. 3, pp. 127–239, 2014.

[14] Y. Sun, P. Babu, and D. P. Palomar, "Majorization-minimization algorithms in signal processing, communications, and machine learning," *IEEE Trans. Signal Process.*, vol. 65, no. 3, pp. 794–816, 2016.

[15] M. Hong, T.-H. Chang, X. Wang, M. Razaviyayn, S. Ma, and Z.-Q. Luo, "A block successive upper-bound minimization method of multipliers for linearly constrained convex optimization," *Mathematics of Operations Research*, vol. 45, no. 3, pp. 833–861, 2020.

[16] J. Song, P. Babu, and D. P. Palomar, "Sequence design to minimize the weighted integrated and peak sidelobe levels," *IEEE Trans. Signal Process.*, vol. 64, no. 8, pp. 2051–2064, 2015.